SEA SURFACE SPECTRUM RETRIEVAL FROM SENTINEL-2 SUN GLITTER IMAGERY

Maria Yurovskaya[1], Vladimir Kudryavtsev[1,2], Bertrand Chapron[3], Fabrice Collard[4]
[1]Marine Hydrophysical Institue RAS (MHI), Kapitanskaya st., 2, 299011, Sevastopol, Russia
Email: mvkosnik@gmail.com@gmail.com
[2]Russian State Hydrometeorological University (RSHU), Malookhtinsky prospect 98, 195196, Saint-Petersburg, Russia
E-mail: kudr@rshu.ru
[3]Institute Francais de Recherche pour l'Exploitation de la Mer, Centre de Bretagne - BP 70 – 29280, Plouzané, France
E-mail: bertrand.chapron@ifremer.fr
[4]Ocean Data Laboratory (ODL), Brest, France
E-mail: dr.fab@oceandatalab.com

KEY WORDS: satellite imagery, sun glitter, Sentinel-2, surface wave spectrum

ABSTRACT: A method is proposed to retrieve directional spectra of the surface waves using satellite sun glitter imagery.Image brightness variations are converted into the sea surface elevations using the transfer function determined from the smoothed shape of the sun glitter. The technique is applied to Sentinel-2 multi-spectral images. Due to specific instrumentation and configuration of multi-channel detectors, Sentinel-2 data enable to determine (i) the surface brightness gradients in sensor zenith and sensor azimuth directions and (ii) space-time characteristics of the surface waves using time delay in cross-channel measurements. As shown, the latter can be used both to remove directional ambiguity in 2D spectra and to get dispersion relation for the surface waves. Directional spectra derived from Sentinel-2 sun glitter imagery are compared with in situ buoy measurements. A fairly good agreement of the sun glitter wave spectra with in situ measurements is found.

1. INTRODUCTION

Ocean color studies are the main oceanographic applications of satellite optical data measurements. In this context the sunlight reflected from the sea surface provides significant difficulties to retrieve the ocean color parameters. On the other hand, sun glitter contains valuable information on statistical properties of the sea surface roughness, its mean square slope (MSS), skewness and kurtosis, as had been originally demonstrated by Cox and Munk (Cox, Munk, 1954), and later in number of succeeding studies (e.g. Bréon and Henriot, 2006). .

The upper ocean dynamic processes affect the sea surface roughness MSS, and thus becomes "visible" through local modulations of the sun glitter brightness. As examples: Hennings et al. (1994) described the surface manifestation of shallow water bottom topography in sun glitter brightness, Apel et al. (1975) and Artale et al. (1990) observed and studied non-linear internal waves in sun glitter imagery, Jackson (2007) investigated distribution of internal waves over the global ocean using MODIS sun glint imagery. Satellite sun glitter imagery of surface slicks have been studied and reported in many papers (e.g. in Adamo et al., 2005; Hu et al., 2009). Kudryavtsev et al. (2012a, 2012b) suggested an approach to convert sun glitter brightness variations into the MSS anomalies and applied this approach to quantify satellite observations of oil spills and meso-scale ocean currents.

Local modulations of the surface slopes associated with long surface waves (swell and spectral peak of wind-generated waves) lead to corresponding variations of the sun glitter brightness. Airborne photography of the sun glitter provides information on 2D field of the surface brightness. In this case long wave induced modulation of the sun glitter brightness can effectively be converted into the 2D spectra of the surface elevations, as it was suggested in the past (see e. g. Stillwell, 1969; Bolshakov et al., 1988, 1990a). Bolshakov et al. (1990b) exploited the airborne sun glitter imagery to investigate development of 2D wind wave spectra with the fetch, and transformation on the surface wave field on the Black Sea currents.

Contrary to airborne photography, satellite optical scanners normally provide measurements of the surface brightness in one direction, like e.g. in case of MERIS, where the measurements are performed in cross-track direction, hence the measured brightness is a function of sensor zenith/incidence angles, and the azimuth sweep is executed due to the sensor movement. Such a technical specificity leads to serious constraints in application of satellite measurements for investigation of the ocean processes (see e.g. Kudryavtsev et al., 2012a for more discussion).

Due to specific instrumentation and configuration of multi-channel detectors, optical scanner on the board of Sentinel-2 enables to determine the surface brightness gradients in two directions, - in sensor zenith and sensor azimuth directions. Moreover, time delay between the cross-channel measurements provides additional opportunity

to study space-time variability of observed surface wave field. These factors, together with high ground resolution, (e.g. 10 m in channels B04 and B08), open unique opportunity to use the developed methods of 2D surface wave spectra retrieval from airborne sun glitter photography to Sentinel-2 data processing.

The goal of this paper is to implement the method of 2D spectra retrieval from sun glitter imagery for Sentinel-2 data processing, and to validate suggested approach against in situ buoy measurements. Though this study is focused on Sentinel-2 observations, application of the techniques to the analysis of sun glitter images received from other satellite sensors is straightforward.

2. DIRECTIONAL WAVE SPECTRUM RETRIEVAL

Satellite optical images collected during the daylight period contain distinct bright areas of reflected sunlight over the oceans in the region of Sun specular reflection points. These sun glitter regions, where standard ocean color products cannot usually be retrieved, can be more favorable for detecting and investigation of the different upper ocean and surface processes which affect the sea surface MSS and hence generate coherent surface manifestations which are visible in sun glitter images. To sense the surface roughness variations, the red channel is the most preferable one, as the light in this channel is absorbed within a "thin" surface layer and, thus, is not too sensitive to the optical properties of the upper water column.

We consider the surface brightness field in the sun glitter area where the impact of the sky radiance reflected from the surface is negligible. Following Cox and Munk (1954) the sun glitter radiance, *B*, generated by specular reflection of the sun light is given by

$$B = \frac{\rho E_s}{4\cos\theta_v \cos^4\beta} P(Z_1, Z_2) \tag{1}$$

where E_s is the solar irradiance, ρ is the Fresnel reflection coefficient, θ_v is the view zenith angle, P is the 2D probability density function (PDF) of the sea surface slopes z_1 and z_2 in two orthogonal directions x_1 and x_2 correspondingly. Capital Z_1 and Z_2 in (1) denote the sea surface slopes satisfying the conditions of specular reflections of the sun light received by the sensor:

$$Z_1 = -\frac{\sin\theta_s \cos\varphi_s + \sin\theta_v \cos\varphi_v}{\cos\theta_s + \cos\theta_v}$$
$$Z_2 = -\frac{\sin\theta_s \sin\varphi_s + \sin\theta_v \sin\varphi_v}{\cos\theta_s + \cos\theta_v} \tag{2}$$

where θ_s is the sun zenith angle, φ_v and φ_s are the view and sun azimuth angles, correspondingly, and $\tan\beta = \sqrt{Z_1^2 + Z_2^2}$.

Tilts of swell and wind waves of the spectral peak result in the sun glitter brightness variations on the scale of modulating long waves. Notice that long surface waves also tilt and modulate shorter waves possessing most of the surface MSS, that also leads to the brightness modulation. In the context of the present study, this is a disturbing factor which is neglected. Thus, (1) can be represented in a form

$$B \equiv B\cos\theta_v = B(Z_1 + \varsigma_1, Z_2 + \varsigma_2) \tag{3}$$

where (ζ_1, ζ_2) is the slope of long wave. Linearization of (3) gives

$$\tilde{B} = B - B_0 = \frac{\partial B}{\partial Z_j}\varsigma_j \equiv G_{zj}\varsigma_j \ . \tag{4}$$

Here B_0 is the mean brightness field or the sun glitter brightness in absence of long wave modulations, subscript j varies from 1 to 2. Equation (4) in the Fourier space reads

$$\hat{B}(\mathbf{K}) = G_{zj}K_j\hat{\varsigma}(\mathbf{K}) \tag{5}$$

where hat over a variable denotes its Fourier transform. Spectrum of dominant waves, $S(\mathbf{K})$, derived from the

spectrum of sun glitter brightness variations, $S_B(\mathbf{K})$, apparently follows from (5) and reads

$$S(\mathbf{K}) = S_B(\mathbf{K})/(G_{zj}K_j)^2 . \quad (6)$$

This relation contains singularity around $G_{zj}K_j = 0$ where retrieval of the wave spectrum is impossible. As a first guess it can be removed assuming that narrow sector of $\hat{B}(\mathbf{K})$ embracing the line $G_{zj}K_j = 0$, does not contribute to the elevation field.

To derive the gradients G_{zj} in (4)-(6) let's represent the "observed" sun glitter gradients, $G_i = \frac{\partial B}{\partial x_i}$, in a form

$$G_i = \frac{\partial B}{\partial Z_j}\frac{\partial Z_j}{\partial x_i} = G_{zj}\frac{\partial Z_j}{\partial x_i} . \quad (7)$$

Then the gradients G_{zj} can be obtained as:

$$\begin{aligned} G_{z1} &= \left(G_2 Z_{2,1} - G_1 Z_{2,2}\right)/\Delta \\ G_{z2} &= \left(G_1 Z_{1,2} - G_2 Z_{1,1}\right)/\Delta \end{aligned} \quad (8)$$

where $Z_{i,j} = \frac{\partial Z_i}{\partial x_j}$ and Δ is determinant defined by $\Delta = Z_{1,2}Z_{2,1} - Z_{1,1}Z_{2,2}$.

This approach is self-consistent. The mean (averaged over dominant waves scale) 2D shape of the sun glitter brightness, $B_0(x_1,x_2)$, defines the gradients G_{zj} by (8) which are then used for conversion of the brightness variation spectrum, $S_B(\mathbf{K})$, into the wave elevation spectrum, $S(\mathbf{K})$, following eq. (6).

3. METHOD APPLICATION

3.1 Sentinel-2 images in sun glitter area

The Sentinel-2 image is formed by 12 arrays of detectors, which cover the whole field of view. The odd arrays are looking forward, and the even arrays are looking backward. Therefore, there is the azimuth difference between successive arrays, and hence the image is "striped" if brightness of observed surface varies with azimuth (like in sun glitter). For the goal of the present study we use the red or near infra-red channels: B04, B08 (0.665 μm and 0.842 μm, respectively, at 10 m resolution), and B8A (0.865 μm at 20 m resolution). As mentioned, usage of this band is preferable for the sun glitter imagery of the surface roughness, since red light does not penetrate to the water column and thus is less affected by a spatial variability of the ocean "color".

Example of the Sentinel-2 "striped" granule (also called tile) in sun glitter area in front of South Africa coast is shown in Fig. 1. Due to some satellite orbit inclination the strips in ortho-images (Level-1C product) are also inclined. For further simplicity we rotate the image and direct x_1- and x_2-axis perpendicular and along the track (or the strips), respectively, like in Fig 1, *b*.

Sensor incidence and azimuth angles shown in Fig. 2, *a*, *b* document that brightness strips originate from step-like change of the sensor azimuth. Such a "defect" of Sentinel-2 imagery provides information on brightness gradient both in incidence and azimuth directions, and thus opens unique opportunity to retrieve surface wave spectra using sun glitter imagery described in the section above. For given sun and sensor angles, surface slopes providing specular reflections, $Z_n = \sqrt{Z_1^2 + Z_2^2}$, vary from 0.17 to 0.21 (Fig. 2, *c*) that corresponds to MSS values at winds 5-7 m/s (Cox and Munk, 1954). Though we do not possess the precise information about the wind field over the area of observation, it is reasonable to expect that parameter Z_n / MSS is close to 1, thus providing optimal conditions

for the surface wave spectra retrieval.

Distribution of the surface brightness inside the box indicated in Fig.1, *b* is shown in Fig. 2, *d*. The brightness field demonstrates pronounced trend in zenith directions, - increasing of *B* with zenith angle within an individual strip along x_1-axis, and abrupt change of *B* at given x_1, where azimuth angle switches from one to other value. Mean brightness field is used to calculate mean brightness gradients, $G_1 = \partial B / \partial x_1$ and $G_2 = \partial B / \partial x_2$. G_1 is defined as the incline of the line approximating mean brightness signal inside each strip, while G_2 is a "jump" on the border of the strips (Fig. 2, *e*).

Then determination of the transfer function components, G_{zj}, following (8), is straightforward. Example of calculations of G_{zj} is shown in Fig. 2, *f*.

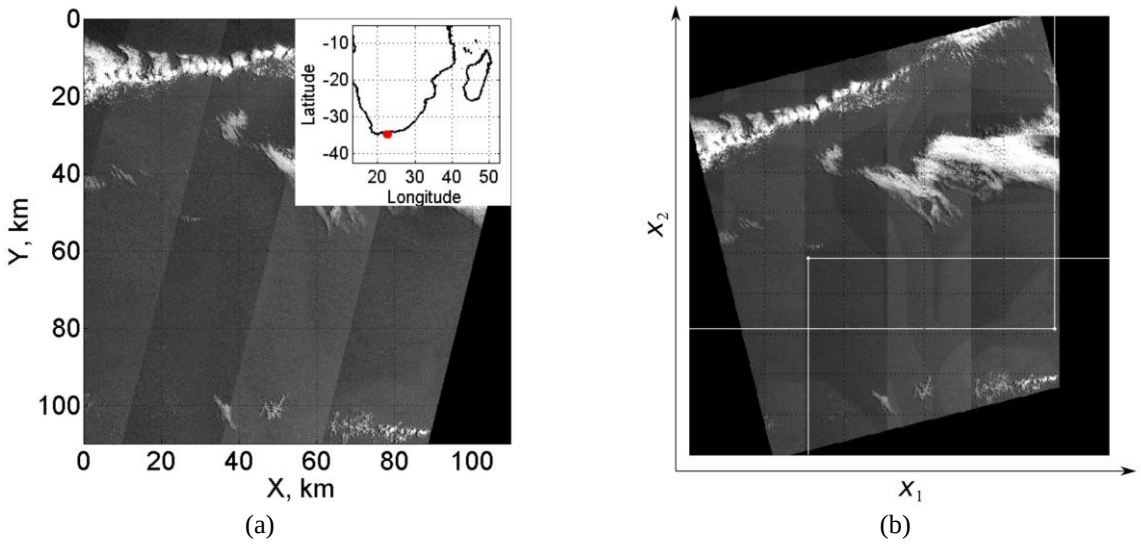

Figure 1. *(a) Sentinel-2 image in channel B04 of the ocean coastal area in front of South Africa on 2016-01-04, 08:13 UTC (S2A_OPER_MSI_L1C_TL_SGS__20160104T141130_A002792_T34HFG_B04.jp2). (b) Rotated image with the selected area of interest marked by white rectangle.*

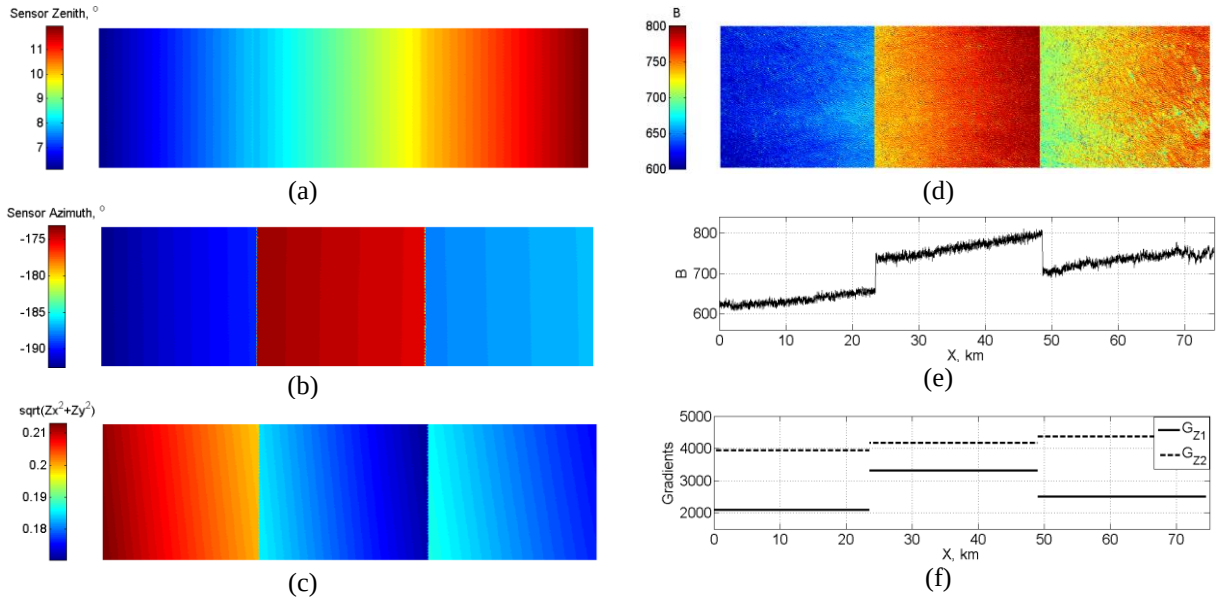

Figure 2. *Sensor zenith (a) and azimuth (b) angles for the image fragment shown in Fig. 1, b in B04 band; parameter* $Z_n = \sqrt{Z_1^{\,2} + Z_2^{\,2}}$ *(c); surface brightness field (d); brightness field averaged over 100 horizontal lines inside the rectangle (e) and components of the tilt transfer function,* G_{z1} *and* G_{z2} *(f).*

3.2 Wave spectrum

Image fragments after brightness trend removal inside each of three stripes in Fig. 2 are presented in Fig. 3, *a*. All respective brightness spectra, Fig. 3, *b*, contain two spectral peaks corresponding to the wave systems travelling in close directions (with 180^o ambiguity) at about 30^o-60^o. Visual inspection of Fig. 3, *a*, confirms the existence of such waves. Wave elevation spectra calculated with use of brightness spectrum (Fig. 3, *b*) and the gradients G_{zj} (Fig. 2, *f*) as input parameters (Eq. 6), are shown in Fig. 3, *c*. As discussed, there is a singularity in the vicinity of $G_{zj}K_j = 0$, where retrieval of the wave spectrum is impossible. Notice that inclination of this line is approximately consistent with sectors of minimal values of the brightness spectrum. Elevation spectra in polar coordinate system after singularity removal (interpolating spectra within the 30^o sector) are presented in Fig. 3, *f*. Application of the transfer function resulted in "redistribution" of the spectral density in **k**-space, and enhancement of the low-wavenumber spectral peak. Respective omnidirectional spectra, $S(k)$, are shown in Fig. 4. Despite some foreseeable difference between three spectra, they all possess two peaks at about 0.025 rad/m and 0.04 rad/m and give close significant wave height (SWH) estimates, $SWH = 4\sqrt{\int S(k)dk}$, listed in figure legend.

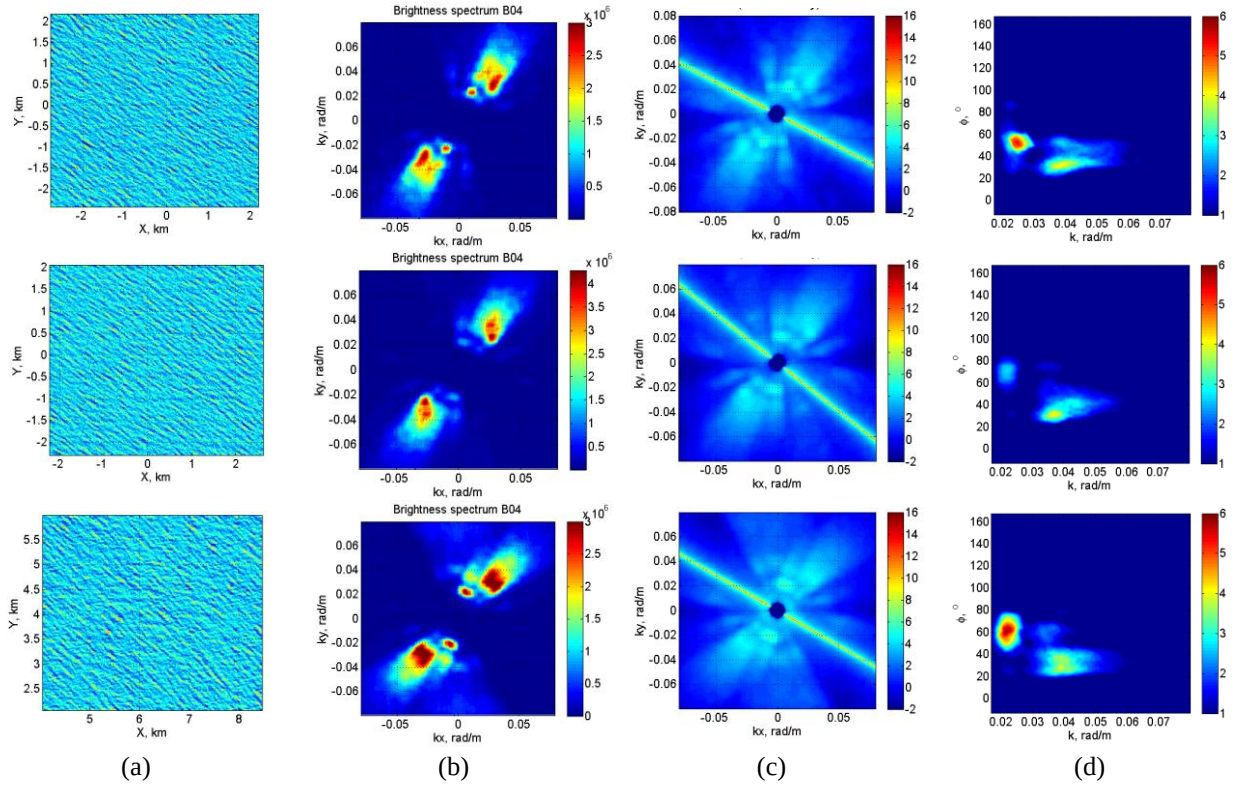

Figure 3. *(a) Image fragments (zoomed parts) inside left (top), central (center) and right (bottom) strips in Fig. 2. (b) Spectrum of the brightness variations. (c) Wave elevation spectrum derived from (6) with singularity at* $G_{zj}K_j = 0$. *(d) Wave elevation spectra in polar coordinates after singularity excision.*

3.3 Directional ambiguity

The above analysis does not give the opportunity to determine the direction of wave propagation (to or from). Nevertheless Sentinel-2 detector configuration allows one to select the true direction between two spectral peaks shifted to 180^0. Three red channels, B04, B08 and B8A, considered in this study, measure the surface at different azimuth angles. Since satellite sensor is moving, the same point on the surface appears in different bands with some time delay. This delay, Δt, can be calculated from satellite passing geometry as

$$\begin{aligned} \Delta t &= D/V \\ D &\approx \Delta\varphi H \tan\theta \end{aligned} \qquad (9)$$

where D is ground distance, H=786 km is altitude of the satellite, V=7440 m/s is its speed, θ is mean (between two channels) zenith angle, and $\Delta\varphi$ is the azimuth difference.

The comparison of sensor azimuths for channels B04, B08 and B8A is plotted in Fig. 5. The most pronounced azimuth shift, up to 10^{o}, corresponding to 1.8 s time delay, is detected in B08 and B8A bands, while in B04, B08 it is about 3^{o}-5^{o} (0.75 s). Cross-channel time delay can be used to remove, at least, directional ambiguity, and, at best, to calculate dispersion relation of the surface waves.

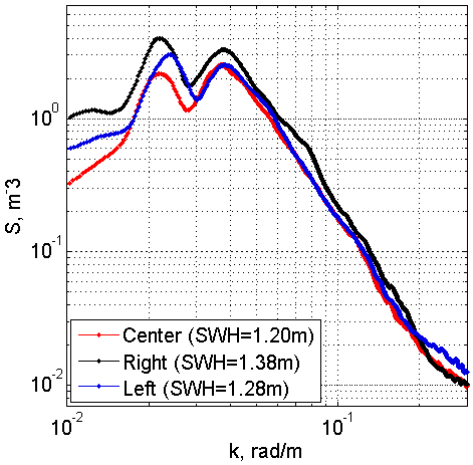

Figure 4. *Omnidirectional elevation spectra for image fragments in Fig. 3.*

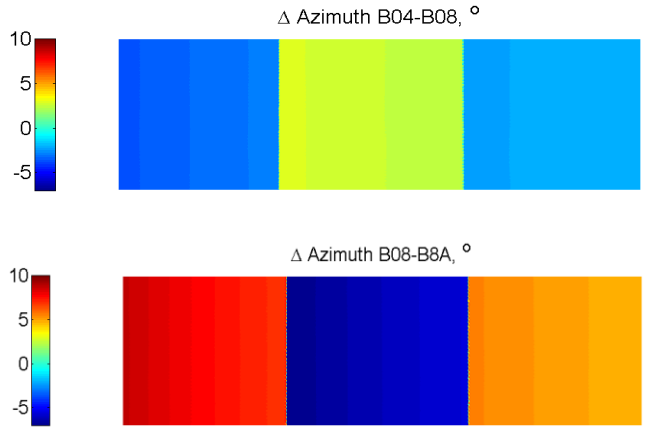

Figure 5. *Azimuth difference between bands B04, B08 (top) and B08, B8A (bottom) inside rectangular image fragment in Fig. 1, b.*

Spectra of coherence and phase derived from cross-spectrum of brightness field in mentioned channel combinations are shown in Fig. 6, *a*, *b*. The images are highly correlated that is confirmed by high coherence level in spectral domain possessing the energy of brightness variations. Phase spectrum has 180-degree asymmetry revealing space-time origin of observed wave field. Anticipated phase shift following from the linear wave theory (Fig. 6, *c*) are estimated as

$$\Phi(k) = -\omega\Delta t = -\sqrt{gk}\Delta t \tag{10}$$

The domains in **k**-space where measured phase is close to the predicted one indicate what spectral wave components are "true" (the waves go from). Spectral behavior of measured phase minus model phase, calculated using (10) is shown in Fig. 6, *d*. It is similar in both channel combinations: waves propagate from open ocean, south-east to the African coast.

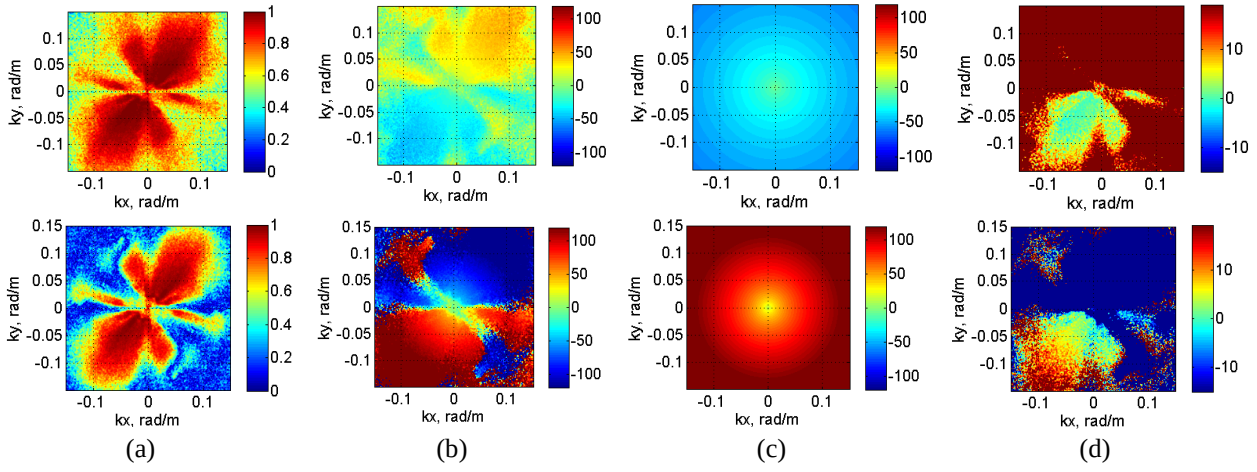

Figure 6. *(a) Spectra of coherence (a) and phase spectra (b) obtained from cross-spectrum of channel B04, B08 (top) and B08, B8A (bottom). (c) Phase shift prediction according to the linear theory (10). (d) The difference between the observed phase and the model one; the spectral domain where the difference is close to 0 indicates the "true" direction of wave components.*

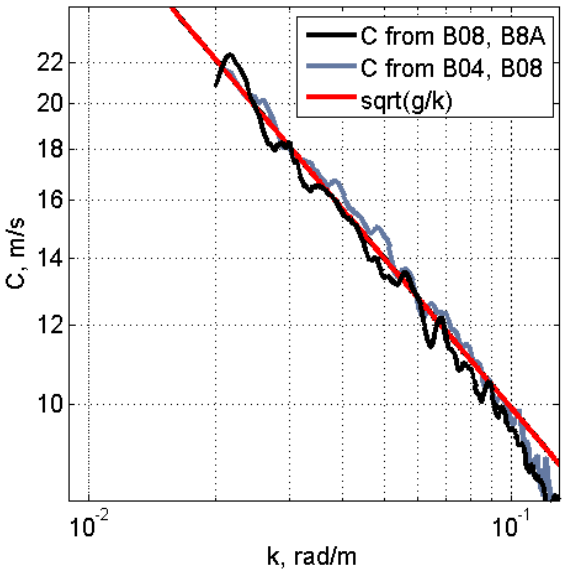

Figure 7. *Dispersion relation, C(k), derived from cross-channel analysis against the model linear relation,* $C = \sqrt{g/k}$.

Besides the qualitative elimination of the directional ambiguity, the quantitative analysis of wave phases can be performed, as they are in a quite good relation with the model predictions. Transects of the cross channel phase, $\Phi(k,\varphi)$, represented in terms of phase velocity, $C = \Phi(k,\varphi_m)/(k\Delta t)$, in maximum coherence direction, are shown in Fig. 7. They agree well with the linear dispersion relation of the surface gravity waves in absence of current.

4. COMPARISON WITH IN SITU DATA

Below we compare reconstructed "sun glitter" spectrum with in situ buoy-measurements. Sentinel-2 image used to validate the method was acquired near the buoy in front of Florida on 2016-05-14 16:04 (Fig. 8). The details of the image processing are the same as described above. Directional buoy and "sun glitter" spectra are compared in Fig. 9, *a, b*. The latter spectrum is the "true" directional spectrum obtained from the folded spectrum by applying the mask taken from the difference between observed and model phase spectra (1 if this difference is less than 15° and 0 in opposite case). Elevation spectrum has a broad angular distribution with mean direction coinciding with visually observed wave direction in Fig. 8, *b*. As compared to the buoy spectrum, sun glitter spectrum has much higher directional resolution.

Omnidirectional sun glitter spectrum, Fig. 9, *c*, is also consistent with the buoy one. It has the similar spectral level and shape, even reproducing high-frequency secondary spectral peak around *k*=0.15 rad/m. SWH calculated from sun glitter spectrum, *Hs*=1.2 m, is very close to that measured by the buoy.

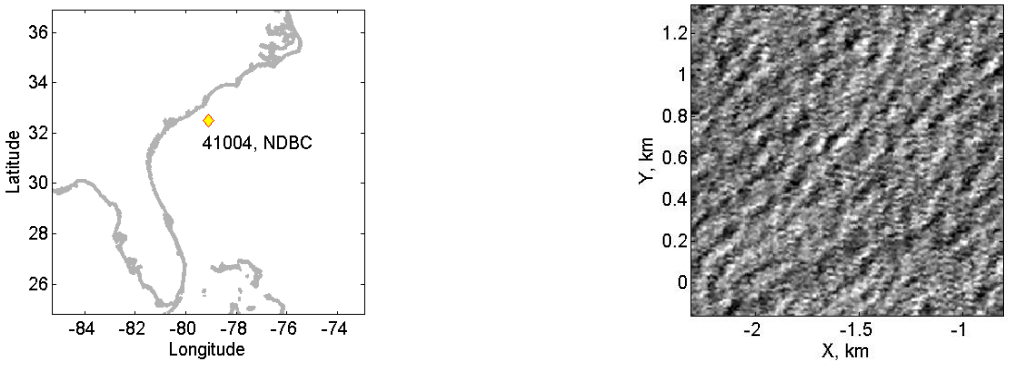

(a) (b)

Figure 8*. (a) Buoy location (41004 - Edisto, owner is National Data Buoy Center) and (b) fragment of Sentinel-2 image (S2A_OPER_MSI_L1C_TL_MTI__20160514T210835_A004670_T17_RNM_B04.jp2) near the buoy.*

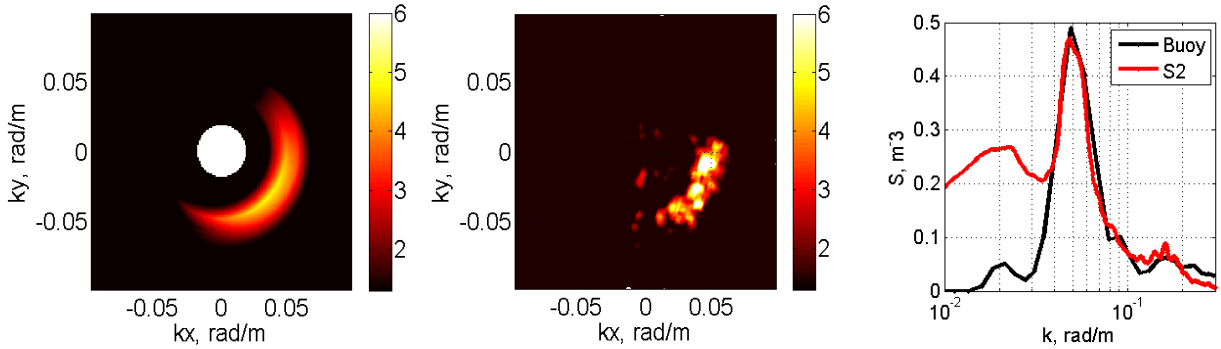

Figure 9*. (a) 2D wave elevation spectrum from buoy data; (b) wave elevation spectrum from sun glitter Sentinel-2 image; (c) omnidirectional spectrum comparison.*

5. CONCLUSION

We consider a method of retrieval of the dominant surface wave directional spectra using satellite sun glitter imagery. Observed image brightness modulations are converted into the sea surface elevations using a transfer function determined from the smoothed shape of the sun glitter. The method is applied to Sentinel-2 multi-channel images. Owing to specific instrumentation and configuration of detectors, Sentinel-2 data gives the surface brightness gradients in two perpendicular directions. Space-time characteristics of the surface waves are retrieved using time delay in cross-channel measurements. The small temporal lag in any pair of bands, B04, B08 and B8A, can be exploited both to remove directional ambiguity in 2D spectra and to get dispersion relation for the surface waves.

Directional spectra derived from Sentinel-2 sun glitter imagery are compared with in situ measurements from the buoy. Sun glitter spectra reproduce direction of waves, shape of the measured omnidirectional spectra, and significant wave height. A fairly good agreement of the retrieved wave spectra with in situ measurements is found. Results of this study suggest that S2 measurements can be used for development of new satellite product, - surface wave spectra, which can further be applied to investigate the ocean surface wave field evolution on global scales.

Acknowledgements. The authors gratefully acknowledge funding by Russian Science Foundation under grant 15-17-20020 to support this study. The used data are available at: https://scihub.copernicus.eu/dhus/#/home (Sentinel-2 data) and http://www.ndbc.noaa.gov/ (buoy measurements).

REFERENCES

Adamo, M., G. De Carolis, V. De Pasquale, and G. Pasquariello, 2005. Combined use of SAR and MODIS imagery to detect marine oil spills, SAR Image Analysis, Modeling, and Techniques VII. Edited by Posa, Francesco, Proceedings of the SPIE, Volume 5980, pp. 153-164.

Apel, J. R., H. M. Byrne, J. R. Proni, and R. L. Charnell, 1975. Observation of oceanic internal and surface waves from the Earth Resources Technology Satellite. J. Geophys. Res., 80, pp. 865-881

Artale, V., D. Levi, S. Marullo, and R. Santoleri, 1990. Analysis of Nonlinear Internal Waves Observed by Landsat Thematic Mapper. J. Geophys. Res., 95(C9), pp. 16,065–16,073.

Bréon, F. M., and N. Henriot, 2006. Spaceborne observations of ocean glint reflectance and modeling of wave slope distributions. J. Geophys. Res., 111(C06005), doi:10.1029/2005JC003343.

Cox, C., and W. Munk, 1954. Measurement of the roughness of the sea surface from photographs of the Sun's glitter. J. Opt. Soc. Amer., 44, pp. 838–850.

Hennings, I., J. Matthews, and M. Metzner, 1994. Sun glitter radiance and radar cross-section modulations of the sea bed. J. Geophys. Res., 99(C8), pp. 16,303–16,326.

Hu, C., X. Li, W. G. Pichel, and F. E. Muller-Karger, 2009. Detection of natural oil slicks in the NW Gulf of Mexico using MODIS imagery. Geophys. Res. Lett., 36(L01604), doi:10.1029/2008GL036119.

Jackson, C., 2007. Internal wave detection using the Moderate Resolution Imaging Spectroradiometer (MODIS), J. Geophys. Res., 112(C11012), doi:10.1029/2007JC004220.

Kudryavtsev V., A. Myasoedov, B. Chapron, J. Johannessen, F. Collard, 2012a. Joint sun-glitter and radar imagery of surface slicks, Remote Sensing of Environment, 120, pp. 123-132, doi:10.1016/j.rse.2011.06.029

Kudryavtsev V., A. Myasoedov, B. Chapron, J. Johannessen, and F. Collard, 2012b. Imaging meso-scale upper ocean dynamics using SAR and optical data, J. Geoph. Res., 117(C04029), doi:10.1029/2011JC007492

Stilwell, D., 1969. Directional energy spectra of the sea from photographs, J. Geophys. Res., 74, pp. 1974–1986.